Letter

Origin of the different electronic structure of Rh- and Ru-doped Sr$_2$IrO$_4$

Véronique Brouet,[1] Paul Foulquier ©,[1,2] Alex Louat ©,[1] François Bertran ©,[3] Patrick Le Fèvre,[3]
Julien E. Rault,[3] and Dorothée Colson[2]

[1]*Université Paris-Saclay, CNRS, Laboratoire de Physique des Solides, 91405 Orsay, France*
[2]*Université Paris-Saclay, CEA, CNRS, SPEC, 91191 Gif-sur-Yvette, France*
[3]*Synchrotron SOLEIL, L'Orme des Merisiers, Saint-Aubin-BP 48, 91192 Gif sur Yvette, France*

One way to induce insulator-to-metal transitions in the spin-orbit Mott insulator Sr$_2$IrO$_4$ is to substitute iridium with transition metals (Ru, Rh). However, this creates intriguing inhomogeneous metallic states, which cannot be described by a simple doping effect. We detail the electronic structure of the Ru-doped case with angle-resolved photoemission and show that, in contrast to Rh, it cannot be connected to the undoped case by a rigid shift. We further identify bands below E_F coexisting with the metallic ones that we assign to nonbonding Ir sites. We rationalize the differences between Rh and Ru by a different hybridization with oxygen, which mediates the coupling to Ir and sensitively affects the effective doping. We argue that the spin-orbit coupling does not control either the charge transfer or the transition threshold.

Inducing a metal-insulator transition (MIT) in correlated systems is a major way to reveal new and exotic electronic states [1]. After a decade of study of the spin-orbit Mott insulator Sr$_2$IrO$_4$, it has proved difficult to reach good metallic states, either by doping, beyond the first attempts [2], or by pressure [3]. Substitutions of Ir with 4d transition metals (TM) induces a metallic state but also raises many question about the role of disorder. Which is the main driving force of the MIT, either reduced spin-orbit coupling (SOC) [4] or effective doping [5], has recently been challenged again by an Angle resolved photoemission spectroscopy (ARPES) study in favor of SOC [6]. X-ray absorption spectroscopy [5,7] and ARPES [8,9] have shown that, unexpectedly, Rh, isovalent to Ir, dopes holes into Sr$_2$IrO$_4$, as if its energy levels were below those of Ir (see Fig. 1). In contrast, Ru, which has one more hole than Ir, does not seem to dope at low values [10,11], suggesting an opposite hierarchy between energy levels. In this situation, Ru should transfer electrons to Ir, but this is forbidden by the Coulomb repulsion on Ir, as long as the insulating Mott state resists. To complicate things further, the atomic Coulomb repulsion U is at least as strong for Ru and Rh as for Ir and the metallic states found in Sr$_2$RuO$_4$ and Sr$_2$RhO$_4$ are only understood by their smaller SOC that preserves the degeneracy of the conduction band, which reduces the impact of correlations [12,13]. Hence, there is a strong interdependence between the possibility of charge transfer on Ir, the existence of a Mott state and the effective value of SOC, which makes the problem highly nontrivial, as all these parameters may change through doping.

Sr$_2$Ir$_{1-x}$Ru$_x$O$_4$ remains isostructural up to $x = 0.55$, with a slight decrease of the in-plane rotation of the oxygen octahedra [14]. An insulator-to-metal transition was observed around x $\simeq 0.4$ by transport [14], in concomitance with the disappearance of the long-range magnetic order [15]. A similar behavior was observed in Ru-doped Sr$_3$Ir$_2$O$_7$ [11,16].

The substitution value to reach MIT is much larger for Ru than Rh ($x \simeq 0.1$) and was suggested to correspond to percolation of Ru-rich metallic puddles [11,17]. Nevertheless, the only ARPES study available to date reveals a Fermi surface (FS) containing $5 - x$ electrons at $x = 0.4$, as if a simple hole doping has been reached [6]. How charge transfer emerges from the phase separation at early dopings has not been explained yet.

We report the evolution of the electronic structure as a function of Ru substitutions with ARPES and detail the Fermi surface (FS) at $x = 0.45$. We show that the MIT is not due to a shift of the Sr$_2$IrO$_4$ bands toward the Fermi level, as was observed for Rh doping [8,9]. Instead, the Sr$_2$IrO$_4$ bands gradually lose weight and a new set of bands appears near the Fermi level, in which effective SOC is much smaller than in the Rh case. This rules out that SOC is the key factor of the MIT. Supported by DFT calculations, we explain the different
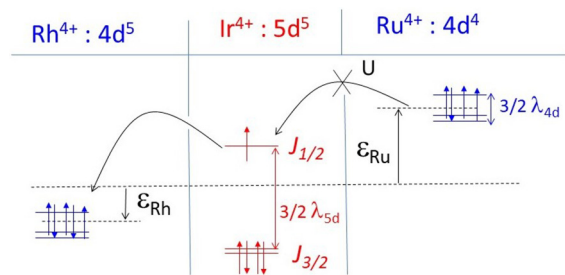
FIG. 1. Sketch of the ionic t_{2g} levels for Rh, Ir, and Ru. SOC splits them into one $J_{1/2}$ and two $J_{3/2}$ levels ($J_{3/2-m_J}$ with $m_J = \pm 1/2, 3/2$), with a much larger value for Ir, being a 5d TM, than Rh and Ru ($\lambda_{5d} \simeq 0.5$ eV vs $\lambda_{4d} \simeq 0.1$ eV). We assume a shift ε between Ir and the other TM (see Fig. 4 for a discussion of its origin). Electrons should be transferred to the lowest available energy level, unless the Coulomb repulsion U forbids double occupation.
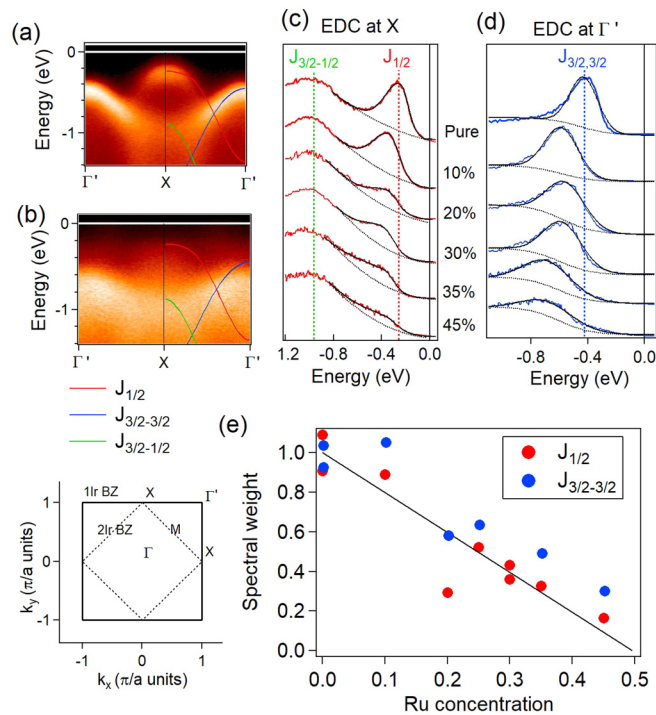
FIG. 2. (a) Energy-momentum plot along $\Gamma'X$ in Sr_2IrO_4 ($k_y = 3$; see Brillouin zone sketch below). The lines highlight the three main bands [19]. (b) Same for Sr_2IrO_4 doped with 45% Ru. (c) EDC at X as a function of Ru doping (as indicated) fitted with a polynomial background (dashed line) and an asymmetric Gaussian (black line). (b) Same at Γ' fitted with a fixed steplike background and a Gaussian. (e) Relative spectral weight of the $J_{1/2}$ and $J_{3/2-3/2}$ peaks compared to the pure, when spectra are normalized to the background intensity. More samples are included than those shown in panels (c) and (d).

FIG. 3. Energy-momentum plot of ARPES intensity measured for $x = 0.45$ at 20 K with 100 eV photon energy and linear horizontal polarization, along (a) ΓX ($k_y = 2$) and (b) ΓM. To enhance the low features near E_F, the image is multiplied by a Fermi step along y, centered at -0.27 eV with width 0.2 eV and amplitude 20. Markers sample the dispersions shown in panels (c) and (d) to ease identification of the different bands. (c) Comparison of the high binding energy bands (black markers) with the dispersion measured in pure Sr_2IrO_4 (lines). The dispersion are extracted either from MDC fits or from local maximum. (d) Comparison of the bands near E_F (color markers) with the dispersion measured in 15% doped Rh [9]. The Rh dipersions are shifted up to match the Ru data by the indicated amounts.

SOC by the dominant Ru character of the bands near E_F, which contrasts with the dominant Ir character of the bands near E_F for Rh doping. We assign this difference to a different hybridization with oxygen.

The samples were prepared using a self-flux method, as reported in Ref. [18]. Their exact doping was estimated by energy dispersion x-ray analysis and the structure checked by single-crystal x-ray diffraction. ARPES experiments were carried out at the CASSIOPEE beamline of the SOLEIL synchrotron, with a SCIENTA R-4000 analyzer, 100 eV photon energy, and an overall resolution better than 15 meV.

Figure 2(a) gives an ARPES view of the bands in the pure compound. The $J_{1/2}$ band peaks at X (red line) and the two $J_{3/2}$ bands respectively at Γ for $J_{3/2-3/2}$ (blue line) and X for $J_{3/2-1/2}$ (green line) (these notations are defined in Fig. 1). For clarity, we only indicate the bands with large ARPES weight in these experimental conditions [19]. In Figs. 2(c) and 2(d), we show the energy distribution curve (EDC) at X and Γ', respectively. In strong contrast with the case of Rh, where all peaks rigidly move to the Fermi level [9], the peaks move here slightly to higher binding energy, by about 0.15 eV for all dopings.

The peaks also seem to broaden and/or lose weight. This is clearer for $J_{1/2}$, in which the intensity can be directly compared to the one of the filled $J_{3/2-1/2}$. We use it as a

background reference (dashed line) and extract the $J_{1/2}$ peak spectral weight by fitting the remaining peak with an asymmetric gaussian. The area normalized to this background is reported in Fig. 2(d) and is consistent with a linear decrease as $1-2x$. The intensity of $J_{3/2-3/2}$ is more difficult to evaluate, because its background is not as well defined. The image in Fig. 2(b) shows that, at 45% Ru, its intensity has indeed weakened, as it became comparable to that of the $J_{3/2-1/2}$. Assuming a steplike background, we obtain a similar decrease of intensity as $J_{1/2}$ in Fig. 2(e).

In a correlated system, it would be natural to find a loss of intensity corresponding to a transfer of spectral weight from an incoherent Hubbard-like band to a coherent band near the Fermi level. However, doping a half-filled band, one would rather expect a $(1-x)$ dependence for the incoherent part weight at small doping x [20]. More puzzlingly, no change would be expected for the $J_{3/2-3/2}$ band, which is completely filled.

In Figs. 3(a) and 3(b), we show the full dispersions at $x = 0.45$ for two high-symmetry directions. We note as black or white markers the bands corresponding to the peaks of Fig. 2. These markers are reported in Fig. 3(c) and compared to the dispersion measured by ARPES in the pure compound [21], to which they are nearly identical. On the other hand, there are three new bands appearing closer to the Fermi level, emphasized as color markers. Two of them cross the Fermi level, as indicated by arrows. They exhibit weak QP peaks but

no pseudogap [19]. The resulting FS [19] is similar to that observed in Ref. [6].

The dispersions of these metallic bands, reported in Fig. 3(d), correspond quite well to the expectation for three t_{2g} bands split by SOC. In particular, the shape of the green band forming an electron-like pocket centered at Γ' is typical of the avoided crossings between d_{xy} and $d_{x^2-y^2}$, observed for $J_{3/2-1/2}$ in compounds where the oxygen octahedra are rotated [22]. This band does not seem to reach the Fermi level. The red band forms a large squarish electron pocket around Γ, containing $n = 0.8$ electrons according to the Luttinger theorem, while the blue band forms smaller squarish pockets around Γ', containing $n = 0.18$ holes [19]. This FS structure looks like the α and β sheets observed in Sr_2RuO_4 [23]. Adding electrons of these three bands, we obtain a total $n = 4.62$ electrons, remarkably close to the $5 - x$ electrons expected for a simple hole doping by Ru. This implies that, despite the coexistence of two sets of bands (insulating-like in black and metallic-like in color), the FS does not correspond to a phase separation between electronically isolated Ir and Ru clusters.

To further characterize the metallic bands, we compare them in Fig. 3(d) with dispersions measured in the other known hole-doped metallic case, at 15% Rh [21]. These models describe well the Ru-doped dispersions, implying there is no significant renormalization. Similarly, there is no significant sharpening of the peak near E_F. From this point of view, Ru-doped Sr_2IrO_4 is similar to other doped Sr_2IrO_4, lacking the traditional fingerprints of a correlated Fermi liquid, contrary to Sr_2RhO_4 [24,25] and Sr_2RuO_4 [26], where renormalizations of factors 2–3 are observed near E_F.

For $J_{1/2}$, the Rh model has to be shifted up by 170 meV, which can be understood from the different fillings (4.55 and 4.85, respectively). However, a huge shift of 0.7 eV is needed for the $J_{3/2-3/2}$ band, which is still 0. 2eV below E_F at Γ for $x_{Rh} = 0.15$. This indicates a highly nonrigid shift between Ru and Rh doping and suggests a drastic reduction of the SOC, which controls the splitting between $J_{1/2}$ and $J_{3/2}$. Indeed, the momentum splitting $\delta k = 0.27\pi/a$ between the two bands at E_F is similar to the one measured in the purely $4d$ Sr_2RhO_4 [22,24]. Extracting a SOC value from the dispersions, however, is difficult, as it could be renormalized [26] or enhanced [27,28] by correlations and also affected by a different closure of the Mott gap in the two cases. Assuming that SOC is a simple average between Ir and the TM dopant, one would expect a 30% stronger reduction for doped Ru for which x is larger, but this hardly explains a value appearing similar to $4d$ metals. A better evaluation would take into account the atomic weight of the bands. Following the hierarchy of energy levels sketched in Fig. 1, one can expect the top of the band to have more Ru character, and hence a SOC more effectively reduced than expected from x and the opposite for Rh doping [19]. The different alignment of energy levels (i.e., on-site energies ε) then gives a qualitative explanation for the difference in SOC in the FS near the MIT.

We now consider possible origins for these different ε. It has been proposed that the smaller SOC leads to electron trapping in Rh [8,29], but Ru does not trap electrons, so it cannot be the only reason. Alternatively, a positive impurity potential was assumed for Ru in Ref. [6], because of its different charge, but this does not explain why Rh hole dopes.
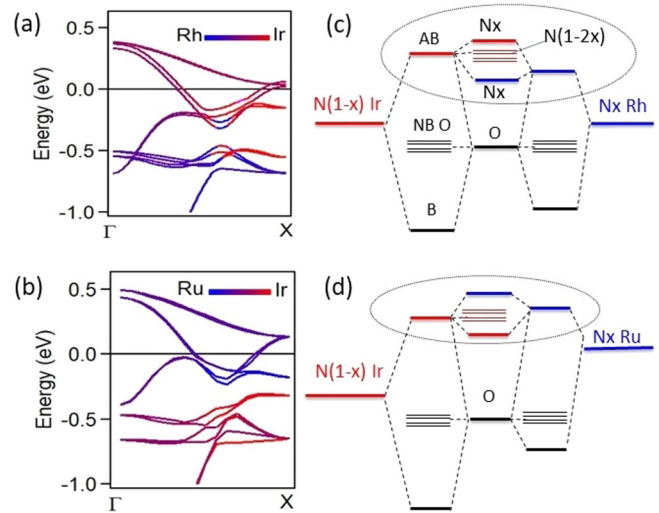
FIG. 4. (a) Band structure calculated for an ordered structure $Sr_2(IrRh)_{0.5}O_4$ along ΓX, without SOC. The color is proportional to the atomic character (red-blue scale). (b) Same for Ru. [(c), (d)] Sketch of the energy levels of oxygen, Ir, and TM dopant and their relative hybridization, based on calculation presented in the Supplemental Material, but not to scale. The hybridized states have mixed atomic character, and their color indicates the dominant one. The circled part represents hybridization of N levels, from Ir and TM.

To get a qualitative idea of how the energy levels could align, we performed DFT calculations for the simplest structure mixing the two atoms, an ordered Sr_2IrO_4 structure with 50% Ir replaced by another TM. As shown in Fig. 4, the distribution of Ir and dopant weight is strikingly different, with more Ru weight on top of the band and more Rh weight at the bottom. The respective contribution are of the order 40–60% at the Fermi level. As SOC is not included here, this suggests that the origin of the difference is rooted in basic properties of the electronic structure.

To some extent, mixing different TM in a compound reproduces locally what happens at oxide heterostructures, where charge transfer is commonly observed as a result of different electronegativity [30] or hybridization strength [31]. Observing different valence states of TM doped in oxides is actually not so uncommon [32,33]. $LaCoO_3$ [32] leads to pairs of Rh^{4+} and Co^{2+} and Mn in $Sr_3Ru_2O_7$ [33] to Mn^{3+} and Ru^{5+}.

As described in Ref. [30], to "align" the energy levels, a natural reference is the oxygen states, which must be shared between the two TM. Following this idea, we present in supplementary DFT calculations evaluations of the coupling with oxygen [19]. The essential results are sketched in Figs. 4(c) and 4(d). Hybridization between oxygen and TM creates antibonding (AB) and bonding (B) states, respectively dominated by the TM and the oxygen, as well as nonbonding (NB) states for oxygens states without TM partners. Their splitting depends both on the coupling strength and the relative initial energy of TM and oxygen [19] and turns out to be significantly smaller for Rh than Ir (4.7 vs 5.4 eV), as could be anticipated from the smaller extension of $4d$ orbitals. This would create an energy difference between Ir and Rh AB levels initially absent. Having one less electron, Ru displays a smaller electronegativity, which destabilizes its initial

energy level compared to O. The calculation suggests this effect nearly compensates for the smaller coupling strength of 4d element and could reverse the respective positions of AB levels.

In the circled part of Fig. 4, we consider the hybridization of N atoms including x TM, starting from these relative positions. This shall create Nx B and Nx AB states with larger atomic character from the closest energy level. The difference in relative position for Ru and Rh induced by coupling to oxygen explains qualitatively the different distributions of atomic character in Figs. 4(a) and 4(b) and, by extrapolation, the tendency of isolated Rh to trap one electron. If there are fewer Rh or Ru atoms than Ir ($x \ll 0.5$), there shall be a corresponding number $N(1-2x)$ of unpaired Ir NB states. As this is exactly the weight we found for the peaks remaining at Ir positions in Fig. 2, it is tempting to identify them with NB-like Ir states. The downshift of 0.15 eV observed with Ru could correspond to a new position of the Fermi level fixed by the AB states, even when their intensity is too small to be detected. It is remarkable that the NB states remain insulating-like, despite the progressive formation of a metallic environment. A full description of the new band structure, taking correlation effects into account, is beyond the scope of this paper, but should be very interesting. We note, for example, that in Fig. 3, the NB $J_{1/2}$ could form a nearly flat band rather than follow the original Sr_2IrO_4 dispersion. The existence of NB states could also solve the puzzle of the pseudogap observed in Rh-doped metallic state [8,9]. We have shown that the pseudogap is not restricted to the region near k_F, but is on the contrary clearest at X, where only incoherent weight is expected [21]. This becomes natural if the pseudogap is due to a distorsion of the line shape near E_F, created by the underlying structure of NB states, that would be for Rh close to the metallic band but possibly remaining distinct.

Recently, Zwartsenberg *et al.* argued that the MIT occurs when the effective SOC reaches a certain threshold ($\lambda = 0.44$ eV) and that it is obtained at a larger x for Ru than Rh, defining a different substitution threshold for the MIT in each case [6]. This seems to be in strong contradiction with our finding that the two metallic states emerge with very different effective SOC, and moreover, are much smaller for Ru than Rh. The problem is that SOC is modulated across the band

structure depending on its atomic content [19]. Upon Ru doping, it is smaller near E_F, as we found for the metallic bands in this paper, and larger at higher binding energy where Ir dominates, as Ref. [6] estimated from ARPES relative orbital intensities. These different estimations are not in contradiction and they are in fact based on the same idea of the influence of the on-site energies ε on the dilution of the effective SOC. Now, regarding the MIT, the common wisdom is that the role of SOC is simply to lift the degeneracy [12,13]. In this respect, whatever the precise SOC value is, the Rh and Ru MIT do not happen at the same effective degeneracy. Therefore, we do not see how the MIT could be controlled by SOC.

In our scenario, the reason for the different doping threshold depends on the way holes are introduced, either in the lower Hubbard band (Rh case) or in AB states generated by the hybridization between Ir and TM (Ru case). The resulting metallic states are very different and it is therefore not surprising that the MIT does not take place at the same doping. In the Rh case, we have even shown recently that holes and electrons coexist near the MIT [34]. In the Ru case, it is necessary to create enough AB states to develop metallicity, which implies having a doping near $x = 0.5$.

To conclude, the electronic structures upon Rh and Ru dopings differ by much more than a different degree of hole doping; they cannot be deduced from each other by a rigid shift. Despite this, the created metals both have a low degree of coherence, as evaluated from the absence of renormalization and no well-behaved quasiparticle peaks. This appears a characteristic of metallic iridates. This study further gives a vivid example of how carriers can be trapped or created at different sites in iridates. We argue that this is due to differences in energy levels arising from different local hybridization with oxygen, which may play a particularly important role for 5d systems. This may reorient our way to think about these materials, as similar effects could be expected around oxygen defects (vacancy, local distorsion) or dopants and be crucial to understanding doping.

[1] S. Paschen and Q. Si, Nat. Rev. Phys. **3**, 9 (2021).

[2] M. Ge, T. F. Qi, O. B. Korneta, D. E. De Long, P. Schlottmann, W. P. Crummett, and G. Cao, Phys. Rev. B **84**, 100402(R) (2011).

[3] C. Chen, Y. Zhou, X. Chen, T. Han, C. An, Y. Zhou, Y. Yuan, B. Zhang, S. Wang, R. Zhang, L. Zhang, C. Zhang, Z. Yang, L. E. DeLong, and G. Cao, Phys. Rev. B **101**, 144102 (2020).

[4] J. S. Lee, Y. Krockenberger, K. S. Takahashi, M. Kawasaki, and Y. Tokura, Phys. Rev. B **85**, 035101 (2012).

[5] J. P. Clancy, A. Lupascu, H. Gretarsson, Z. Islam, Y. F. Hu, D. Casa, C. S. Nelson, S. C. LaMarra, G. Cao, and Y.-J. Kim, Phys. Rev. B **89**, 054409 (2014).

[6] B. Zwartsenberg, R. P. Day, E. Razzoli, M. Michiardi, N. Xu, M. Shi, J. D. Denlinger, G. Cao, S. Calder, K. Ueda,

J. Bertinshaw, H. Takagi, B. J. Kim, I. S. Elfimov, and A. Damascelli, Nat. Phys. **16**, 290 (2020).

[7] S. Chikara, G. Fabbris, J. Terzic, G. Cao, D. Khomskii, and D. Haskel, Phys. Rev. B **95**, 060407(R) (2017).

[8] Y. Cao, Q. Wang, J. A. Waugh, T. J. Reber, H. Li, X. Zhou, S. Parham, S.-R. Park, N. C. Plumb, E. Rotenberg, A. Bostwick, J. D. Denlinger, T. Qi, M. A. Hermele, G. Cao, and D. S. Dessau, Nat. Commun. **7**, 11367 (2016).

[9] A. Louat, F. Bert, L. Serrier-Garcia, F. Bertran, P. Le Fèvre, J. Rault, and V. Brouet, Phys. Rev. B **97**, 161109(R) (2018).

[10] R. J. Cava, B. Batlogg, K. Kiyono, H. Takagi, J. J. Krajewski, W. F. Peck, L. W. Rupp, and C. H. Chen, Phys. Rev. B **49**, 11890 (1994).

[11] C. Dhital, T. Hogan, W. Zhou, X. Chen, Z. Ren, M. Pokharel, Y. Okada, M. Heine, W. Tian, Z. Yamani *et al.*, Nat. Commun. **5**, 3377 (2014).

[12] B. J. Kim, H. Jin, S. J. Moon, J.-Y. Kim, B.-G. Park, C. S. Leem, J. Yu, T. W. Noh, C. Kim, S.-J. Oh, J.-H. Park, V. Durairaj, G. Cao, and E. Rotenberg, Phys. Rev. Lett. **101**, 076402 (2008).

[13] C. Martins, M. Aichhorn, L. Vaugier, and S. Biermann, Phys. Rev. Lett. **107**, 266404 (2011).

[14] S. J. Yuan, S. Aswartham, J. Terzic, H. Zheng, H. D. Zhao, P. Schlottmann, and G. Cao, Phys. Rev. B **92**, 245103 (2015).

[15] S. Calder, J. W. Kim, G.-X. Cao, C. Cantoni, A. F. May, H. B. Cao, A. A. Aczel, M. Matsuda, Y. Choi, D. Haskel, B. C. Sales, D. Mandrus, M. D. Lumsden, and A. D. Christianson, Phys. Rev. B **92**, 165128 (2015).

[16] Z. Wang, Y. Okada, J. O'Neal, W. Zhou, D. Walkup, C. Dhital, T. Hogan, P. Clancy, Y.-J. Kim, Y. F. Hu, L. H. Santos, S. D. Wilson, N. Trivedi, and V. Madhavan, Proc. Natl. Acad. Sci. **115**, 11198 (2018).

[17] X. Feng, Y. Deng, and H. W. J. Blöte, Phys. Rev. E **78**, 031136 (2008).

[18] B. J. Kim, H. Ohsumi, T. Komesu, S. Sakai, T. Morita, H. Takagi, and T. Arima, Science **323**, 1329 (2009).

[19] See Supplemental Material at http://link.aps.org/supplemental/10.1103/PhysRevB.104.L121104 for more information on band structure, Fermi surface at 45% Ru doping, effect of SOC in tight-binding model with different on-site energies, and strength of hybridization with oxygen, as well as Refs. [35–38].

[20] A. Georges, G. Kotliar, W. Krauth, and M. J. Rozenberg, Rev. Mod. Phys. **68**, 13 (1996).

[21] A. Louat, B. Lenz, S. Biermann, C. Martins, F. Bertran, P. Le Fèvre, J. E. Rault, F. Bert, and V. Brouet, Phys. Rev. B **100**, 205135 (2019).

[22] B. J. Kim, J. Yu, H. Koh, I. Nagai, S. I. Ikeda, S.-J. Oh, and C. Kim, Phys. Rev. Lett. **97**, 106401 (2006).

[23] A. Damascelli, D. H. Lu, K. M. Shen, N. P. Armitage, F. Ronning, D. L. Feng, C. Kim, Z.-X. Shen, T. Kimura, Y. Tokura, Z. Q. Mao, and Y. Maeno, Phys. Rev. Lett. **85**, 5194 (2000).

[24] F. Baumberger, N. J. C. Ingle, W. Meevasana, K. M. Shen, D. H. Lu, R. S. Perry, A. P. Mackenzie, Z. Hussain, D. J. Singh, and Z.-X. Shen, Phys. Rev. Lett. **96**, 246402 (2006).

[25] J. Kwon, M. Kim, D. Song, Y. Yoshida, J. Denlinger, W. Kyung, and C. Kim, Phys. Rev. Lett. **123**, 106401 (2019).

[26] A. Tamai, M. Zingl, E. Rozbicki, E. Cappelli, S. Riccò, A. de la Torre, S. McKeown Walker, F. Y. Bruno, P. D. C. King, W. Meevasana, M. Shi, M. Radović, N. C. Plumb, A. S. Gibbs, A. P. Mackenzie, C. Berthod, H. U. R. Strand, M. Kim, A. Georges, and F. Baumberger, Phys. Rev. X **9**, 021048 (2019).

[27] G.-Q. Liu, V. N. Antonov, O. Jepsen, and O. K. Andersen, Phys. Rev. Lett. **101**, 026408 (2008).

[28] S. Zhou, K. Jiang, H. Chen, and Z. Wang, Phys. Rev. X **7**, 041018 (2017).

[29] P. Liu, M. Reticcioli, B. Kim, A. Continenza, G. Kresse, D. D. Sarma, X.-Q. Chen, and C. Franchini, Phys. Rev. B **94**, 195145 (2016).

[30] H. Chen and A. Millis, J. Phys.: Condens. Matter **29**, 243001 (2017).

[31] M. N. Grisolia, J. Varignon, G. Sanchez-Santolino, A. Arora, S. Valencia, M. Varela, R. Abrudan, E. Weschke, E. Schierle, J. E. Rault, J.-P. Rueff, A. Barthélémy, J. Santamaria, and M. Bibes, Nat. Phys. **12**, 484 (2016).

[32] S. V. Streltsov, V. V. Gapontsev, and D. I. Khomskii, J. Phys.: Condens. Matter **28**, 086005 (2016).

[33] M. A. Hossain, Z. Hu, M. W. Haverkort, T. Burnus, C. F. Chang, S. Klein, J. D. Denlinger, H.-J. Lin, C. T. Chen, R. Mathieu, Y. Kaneko, Y. Tokura, S. Satow, Y. Yoshida, H. Takagi, A. Tanaka, I. S. Elfimov, G. A. Sawatzky, L. H. Tjeng, and A. Damascelli, Phys. Rev. Lett. **101**, 016404 (2008).

[34] L. Fruchter and V. Brouet, J. Phys.: Condens. Matter **33**, 215602 (2021).

[35] P. Blaha, K. Schwarz, F. Tran, R. Laskowski, G. K. H. Madsen, and L. D. Marks, J. Chem. Phys. **152**, 074101 (2020).

[36] V. Brouet, J. Mansart, L. Perfetti, C. Piovera, I. Vobornik, P. Le Fèvre, F. Bertran, S. C. Riggs, M. C. Shapiro, P. Giraldo-Gallo, and I. R. Fisher, Phys. Rev. B **92**, 081117(R) (2015).

[37] A. de la Torre, S. McKeown Walker, F. Y. Bruno, S. Riccó, Z. Wang, I. Gutierrez Lezama, G. Scheerer, G. Giriat, D. Jaccard, C. Berthod, T. K. Kim, M. Hoesch, E. C. Hunter, R. S. Perry, A. Tamai, and F. Baumberger, Phys. Rev. Lett. **115**, 176402 (2015).

[38] V. Brouet, M. F. Jensen, P.-H. Lin, A. Taleb-Ibrahimi, P. Le Fèvre, F. Bertran, C.-H. Lin, W. Ku, A. Forget, and D. Colson, Phys. Rev. B **86**, 075123 (2012).